# Cooperative Self-Assembly of Double-Strand Conjugated Porphyrin Ladders

**Peter N. Taylor and Harry L. Anderson***

*Contribution from the Department of Chemistry, University of Oxford, Dyson Perrins Laboratory, South Parks Road, Oxford OX1 3QY, U.K.*

*Received August 6, 1999*

**Abstract:** A series of conjugated zinc porphyrin oligomers, from the dimer through to the hexamer, form stable ladder complexes with linear bidentate ligands such as 1,4-diazabicyclo[2.2.2]octane (DABCO) and 4,4′-bipyridyl (Bipy). The $^1$H NMR spectra of these ladders confirm their structures and show how they fray and dissociate in the presence of excess ligand. The thermodynamics of these equilibria were elucidated by spectrophotometric titration, using multivariate global factor analysis, in two different solvents (chloroform and toluene). Ladder formation and dissociation exhibit many indications of positive cooperativity, including all-or-nothing two-state assembly, sigmoidal isotherms, large Hill coefficients, and narcissistic self-sorting. Ladder formation increases the planarity and conjugation, resulting in a reduction in the gap between the highest occupied and lowest unoccupied molecular orbitals.

## Introduction

Biological macromolecules tend to self-assemble into noncovalent multiple-strand arrays.[1] Nucleic acid double-, triple-, and quadruple-helices are the supreme examples.[2,3] Peptides form coiled coils[4] (as in leucine zippers and collagen) and $\beta$-sheets (as in silk), and the phenomenon even extends to polysaccharides.[5] Self-assembly processes of this type are reversible and controlled by thermodynamics. It is difficult to dissect all of the thermodynamic parameters involved, which leads to a motivation for studying simpler synthetic double-strand assemblies. Oligopyridine metal helicates are the most well-studied artificial multiple-strand arrays,[6] and the thermodynamics of their formation has been investigated in detail, but the change in helicate stability with increasing length has not been explored, probably because long helicates become too stable (both thermodynamically and kinetically) for convenient measurement. Bisson and Hunter have investigated the length dependence of the stability of their double-strand "zippers" and found an intriguing nonlinear free energy length dependence.[7] In this paper, we present thermodynamic data on the self-assembly of a series of double-strand porphyrin ladder structures and explore how the stability and cooperativity increase with increasing length, up to the six-rung ladder.

Nature uses multiple-strand formation to increase the conformational rigidity of biopolymers. This enables their shape to be tightly specified by the covalent connectivity of the components. Self-assembly is the algorithm that translates covalent connectivity into tertiary structure. There is scope for transferring this concept from biology to material science, particularly in the context of electronic materials. For example, McCullough *et al*. have shown that formation of multistrand arrays increases the conjugation in polythiophenes,[8] and Charych *et al*. have used the interaction of polydiaceylenes with viruses to change the conjugation in these polymers and thus to achieve colorimetric virus detection.[9] Here, we demonstrate that double-strand formation increases the conjugation in a series of porphyrin oligomers.[10−13] The potentially useful nonlinear optical behavior of these materials is likely to be enhanced by this increased conjugation.[14−16]

Previously, we have demonstrated that a linear zinc porphyrin

* Address correspondence to Dr. H. L. Anderson, University of Oxford, Department of Chemistry, Dyson Perrins Laboratory, South Parks Road, Oxford, UK OX1 3QY, Telephone: +44 1865 275 704. Fax: +44 1865 275 674. E-mail: harry.anderson@chem.ox.ac.uk.

(1) For reviews of self-assembly, see: Lindsey, J. S. *New J. Chem.* **1991**, *15*, 153−190. Whitesides, G. M.; Mathias, J. P.; Seto, C. T. *Science* **1991**, *254*, 1312−1319. Williams, D. H.; Westwell, M. S. *Chem. Soc. Rev.* **1998**, *27*, 57−63.

(2) (a) Neidle, S. *Oxford Handbook of Nucleic Acid Structure*; Oxford University: Oxford, 1998. (b) SantaLucia, J., Jr.; Allawi, H. T.; Seneviratne, P. A. *Biochemistry* **1996**, *35*, 3555−3562.

(3) Hardin, C. C.; Corregan, M. J.; Lieberman, D. V.; Brown, B. A., II. *Biochemistry* **1997**, *36*, 15428−15450.

(4) Su, J. Y.; Hodges, R. S.; Kay, C. M. *Biochemistry* **1994**, *33*, 15501−15510. Lau, S. Y. M.; Taneja, A. K.; Hodges, R. S. *J. Biol. Chem.* **1984**, *259*, 13253−13261. Boice, J. A.; Dieckmann, G. R.; DeGrado, W. F.; Fairman, R. *Biochemistry* **1996**, *35*, 14480−14485.

(5) Bezemer, L.; Ubbink, J. B.; de Kooker, J. A.; Kuil, M. E.; Leyte, J. C. *Macromolecules* **1993**, *26*, 6436−6446.

(6) (a) Pfeil, A.; Lehn, J.-M. *J. Chem. Soc., Chem. Commun.* **1992**, 838−840. (b) Piguet, C.; Bernardinelli, G.; Bocquet, B.; Quattropani, A.; Williams, A. F. *J. Am. Chem. Soc.* **1992**, *114*, 7440−7451. (c) Piguet, C.; Hopfgartner, G.; Bocquet, B.; Schaad, O.; Williams, A. F. *J. Am. Chem. Soc.* **1994**, *116*, 9092−9102. (d) Krämer, R.; Lehn, J.-M.; Marquis-Rigault, A. *Proc. Natl. Acad. Sci. U.S.A.* **1993**, *90*, 5394−5398. (e) Constable, E. C. In *Comprehensive Supramolecular Chemistry*; Sauvage, J.-P., Hosseini, M. W., Eds.; Elsevier: Oxford, 1996; Vol. 9, pp 213−252.

(7) Bisson, A. P.; Hunter, C. A. *Chem. Commun.* **1996**, 1723−1724.

(8) McCullough, R. D.; Ewbank, P. C.; Loewe, R. S. *J. Am. Chem. Soc.* **1997**, *119*, 633−634. Yue, S.; Berry, G. C.; McCullough, R. D. *Macromolecules* **1996**, *29*, 933−939.

(9) Okada, S.; Peng, S.; Spevak, W.; Charych, D. *Acc. Chem. Res.* **1998**, *31*, 229−239.

(10) Work on conjugated porphyrin oligomers has been reviewed recently, see: Anderson, H. L. *Chem. Commun.* **1999**, 2323−2331.

(11) Anderson, H. L. *Inorg. Chem.* **1994**, *33*, 972−981.

(12) Taylor, P. N.; Huuskonen, J.; Rumbles, G.; Aplin, R. T.; Williams, E.; Anderson, H. L. *Chem. Commun.* **1998**, 909−910.

(13) Lin, V. S.-Y.; DiMagno, S. G.; Therien, M. J. *Science* **1994**, *264*, 1105−1111.

(14) LeCours, S. M.; Guan, H.-W.; DiMagno, S. G.; Wang C. H.; Therien, M. J. *J. Am. Chem. Soc.* **1996**, *118*, 1497−1503.

(15) Anderson, H. L.; Martin, S. J.; Bradley, D. D. C. *Angew. Chem., Int. Ed. Engl.* **1994**, *33*, 655−657.

10.1021/ja992821d CCC: $18.00 
Published on Web 11/30/1999

**Scheme 1**

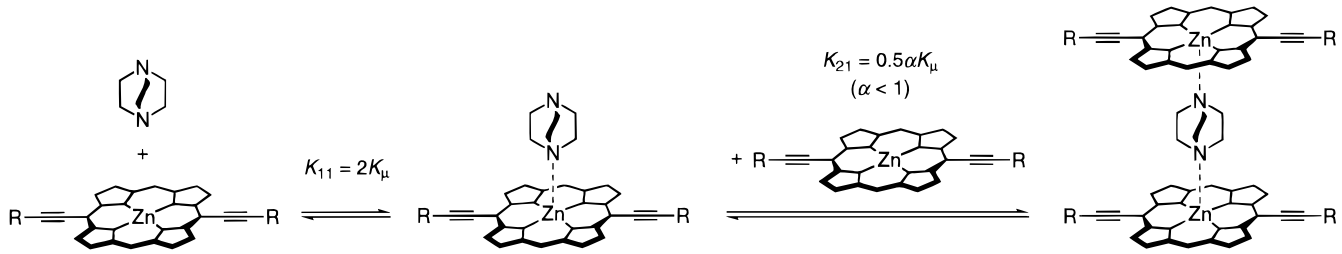


dimer forms a cyclic 2:2 complex (or two-rung ladder) with linear bidentate ligands such as 1,4-diazabicyclo[2.2.2]octane (DABCO) and 4,4′-bipyridyl (Bipy).[11] Discrete complexes are formed because each zinc center coordinates to one ligand, becoming 5-coordinate, whereas a 6-coordinate metal would lead to polymeric arrays. Many supramolecular structures have been assembled using this type of zinc porphyrin−amine coordination.[17] Here, we extend our previous work by investigating the whole series of complexes $\mathbf{1}_2$·DABCO to $\mathbf{6}_2$·$(DABCO)_6$ formed

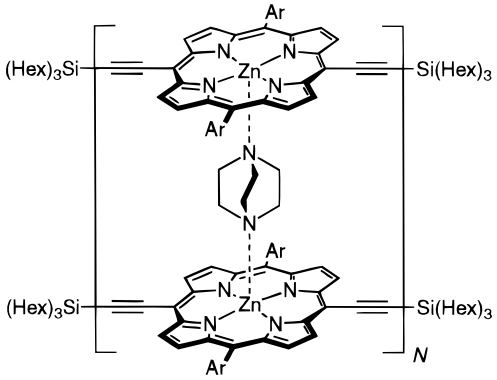

$\mathbf{1}_2$·(DABCO) to $\mathbf{6}_2$·$(DABCO)_6$ ; $N$ = 1 to 6; Ar = 3,5-di(*t*-butyl)phenyl

by the conjugated porphyrin oligomers **1**−**6**.[12] We have used $^1$H NMR and UV−visible titrations to probe the structure and stability of these double-strand arrays. Some of the binding curves are quite complicated and could only be analyzed using multivariate methods which fit a binding model to the whole series of spectra simultaneously.[18] We chose to focus on the DABCO ligand, because its high basicity was expected to lead to particularly stable complexes, but most other linear bidentate ligands would probably behave the same way, and our results suggest that longer ligands such as Bipy may form even more stable ladders than those of DABCO. Compounds **1**−**6** differ from the porphyrins used in our original ladder complexes[11] in that they have *meso*-aryl substituents, which greatly reduces their tendency to aggregate.

## Results and Discussion

**Stability of Nonchelated Complexes.** The difference between self-assembly and simple coordination is that self-assembly processes involve multiple interactions operating in one or more closed loops; the interaction that closes the loop becomes intramolecular, resulting in cooperativity through the chelate effect.[1] Nonchelated multicomponent complexes, in which the interactions do not form a closed loop, do not benefit by this chelative cooperativity, but they may exhibit other types of cooperativity, because coordination to one site of a multidentate ligand can affect the affinity of the other sites (through steric, conformational, or electrostatic communication). Before exploring the self-assembly of ladder structures, we measured the stability of simple complexes, such as those of the porphyrin monomer **1** with the bidentate ligand DABCO and those of the porphyrin oligomers **2**−**6** with a monodentate analogue of DABCO, quinuclidine.

**Table 1.** Binding Constants for Monomer **1** and DABCO

| solvent | $K_{11}/M^{-1}$ | $K_{21}/M^{-1}$ | α |
|---|---|---|---|
| PhMe | $(1.8 \pm 0.2) \times 10^6$ | $(2.7 \pm 0.3) \times 10^3$ | $0.0060 \pm 0.001$ |
| $CHCl_3$ | $(9.9 \pm 1.0) \times 10^4$ | $(4.9 \pm 0.5) \times 10^3$ | $0.20 \pm 0.03$ |

When the coordination of DABCO to **1** is probed by UV−visible titration, only the 1:1 **1**·DABCO complex is formed. Under these dilute conditions (porphyrin concentration $\approx 10^{-6}$ M) there is no significant concentration of the 2:1 complex, $\mathbf{1}_2$·DABCO, so the binding isotherm can easily be analyzed to yield the stoichiometric[19] association constant $K_{11}$ (Scheme 1; Table 1).[20] UV−visible titrations were carried out in two solvents (toluene and chloroform) to compare the behavior under these different conditions. The stronger binding in toluene has been observed previously[21] and can be attributed to its lower dielectric constant and to the ability of chloroform to solvate the ligand by acting as a hydrogen bond donor.[22]

Both the 1:1 and 2:1 complexes are observed when this equilibrium is probed by $^1$H NMR (porphyrin concentration $\approx 10^{-3}$ M). When up to 0.5 equiv of DABCO is added to **1** in $CDCl_3$, unbound **1** and $\mathbf{1}_2$·DABCO are observed in slow exchange. When more than 0.5 equiv of DABCO is added, a fast-exchange equilibrium is established between unbound **1**, $\mathbf{1}_2$·DABCO, and **1**·DABCO (Scheme 1), which gradually shifts

(16) Thorne, J. R. G.; Kuebler, S. M.; Denning, R. G.; Blake, I. M.; Taylor, P. N.; Anderson, H. L. *Chem. Phys.* **1999**, in press. Kuebler, S. M.; Denning, R. G.; Anderson, H. L. *J. Am. Chem. Soc.* **2000**, *122*, in press.

(17) Chi, X.; Guerin, A. J.; Haycock, R. A.; Hunter, C. A.; Sarson, L. D. *J. Chem. Soc., Chem. Commun.* **1995**, 2563−2565; 2567−2569. Anderson, S.; Anderson, H. L.; Bashall, A.; McPartlin, M.; Sanders, J. K. M. *Angew. Chem., Int. Ed. Engl.* **1995**, *34*, 1096−1099. Stibrany, R. T.; Vasudevan, J.; Knapp, S.; Potenza, J. A.; Emge, T.; Schugar, H. J. *J. Am. Chem. Soc.* **1996**, *118*, 3980−3981. Funatsu, K.; Imamura, T.; Ichimura, A.; Sasaki, Y. *Inorg. Chem.* **1998**, *37*, 1798−1804. Reek, J. N. H.; Schenning, A. P. H. J.; Bosman, A. W.; Meijer, E. W.; Crossley, M. J. *Chem. Commun.* **1998**, 11−12.

(18) Malinowski, E. R. *Factor Analysis in Chemistry*, 2nd ed., Wiley-Interscience: New York, 1991. Maeder, M.; Zuberbühler, A. D. *Anal. Chem.* **1990**, *62*, 2220−2224. Gampp, H.; Maeder, M.; Meyer, C. J.; Zuberbühler, A. D. *Talanta* **1986**, *33*, 943−951.

(19) Stoichiometric association constants ($K_{11}$ and $K_{12}$) for multisite ligands are related to microscopic association constants ($K_\mu$) via statistical factors, as indicated in Schemes 1 and 2.

(20) For clarity, Schemes 1−3 and the structure of $\mathbf{5}_2$·$(DABCO)_5$ are drawn with simplified skeletal porphyrins, without aryl substituents.

(21) Walker, F. A.; Benson, M. *J. Am. Chem. Soc.* **1980**, *102*, 5530−5538.

(22) Titrations of **1** and quinuclidine were carried out at a range of temperatures (288, 293, 298, 303, and 308 K) giving linear van't Hoff plots and show that there is dramatic entropy−enthalpy compensation: in toluene, $\Delta H = -61 \pm 4$ kJ mol$^{-1}$ and $\Delta S = -84 \pm 13$ J K$^{-1}$ mol$^{-1}$, whereas in $CHCl_3$, $\Delta H = -31 \pm 4$ kJ mol$^{-1}$ and $\Delta S = -10 \pm 13$ J K$^{-1}$ mol$^{-1}$. The much lower entropy of complexation in chloroform shows that desolvation of the ligand is a significant factor in this solvent.

**Scheme 2**

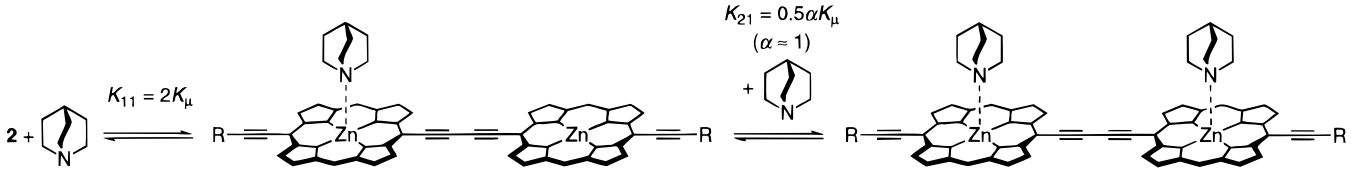


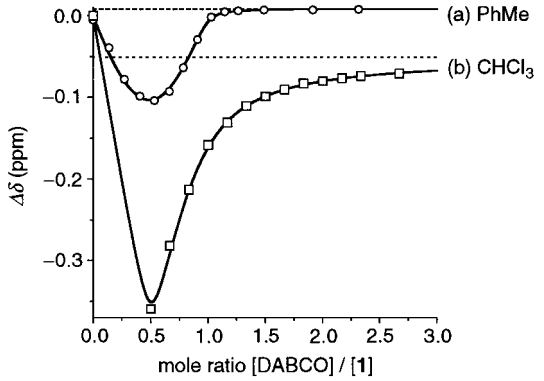


**Figure 1.** $^1$H NMR titration of **1** with DABCO in (a) $d_8$-toluene and (b) $CDCl_3$. $\Delta\delta$ is the average change in chemical shift of the two $\beta$-protons. The smooth curves are calculated from eqs 1−6; dashed lines show values of $\Delta\delta$(**1**·DABCO). In curve b, there are no points in the range 0 < mole ratio < 0.5 because the system is in slow exchange in this region.

toward **1**·DABCO with increasing DABCO concentration. The aromatic and $\beta$-pyrrole protons of **1** are strongly shielded in the $\mathbf{1}_2$·DABCO sandwich complex and return to roughly their original values in **1**·DABCO. When this titration is carried out in $d_8$-toluene, rather than $CDCl_3$, similar behavior is observed, except that the system is in fast exchange throughout the whole titration. Representative curves, from both solvents, are plotted in Figure 1. These data fit well to the calculated curves from eqs 1−6,[23] which follow from Scheme 1. $\delta_M$, $\delta_{M_2L}$, and $\delta_{ML}$ are the chemical shifts of signals from **1**, $\mathbf{1}_2$·DABCO, and **1**·DABCO, respectively; $\delta_{obs}$ is the observed chemical shift.

$$K_{11} = [ML]/[M][L] \quad (1)$$

$$K_{21} = [M_2L]/[ML][M] \quad (2)$$

$$[M]_0 = [M] + [ML] + 2[M_2L] \quad (3)$$

$$[L]_0 = [L] + [ML] + [M_2L] \quad (4)$$

$$K_{11}K_{21}[M]^3 + \{1 + K_{21}(2[L]_0 - [M]_0)\}K_{11}[M]^2 + \{1 + K_{11}([L]_0 - [M]_0)\}[M] - [M]_0 = 0 \quad (5)$$

$$\delta_{obs} = (\delta_M[M] + 2\delta_{M_2L}[M_2L] + \delta_{ML}[ML])/[M]_0 \quad (6)$$

The value of $K_{11}$ was determined independently by UV−visible titration; so, the only unknowns during the analysis of this NMR data were $K_{21}$ and $\delta_{ML}$ (in $CDCl_3$), and $K_{21}$, $\delta_{M_2L}$, and $\delta_{ML}$ (in $d_8$-toluene). Binding constants are shown in Table 1.

The most interesting parameter for this type of equilibrium is the cooperativity between the two binding events, which is quantified by the interaction parameter, $\alpha$, defined by eq 7.[24]

$$\alpha = 4K_{21}/K_{11} \quad (7)$$

In this case, there is negative cooperativity, $\alpha < 1$ (Table 1): coordination to the second nitrogen of DABCO is less favorable than the first. The greater negative cooperativity in toluene is obvious from curve a in Figure 1: the solution of **1** with 1.5 equiv of DABCO in $d_8$-toluene contains no significant concentration of $\mathbf{1}_2$·DABCO, whereas in chloroform, this 2:1 complex survives to higher excesses of DABCO. We have also carried out this titration in $CD_2Cl_2$ and found $\alpha = 0.17$ in this solvent. Previous studies of the interaction of DABCO with metalloporphyrins without *meso*-aryl substituents, in $CD_2Cl_2$ and $CDCl_3$, have concluded that there is rather little cooperativity in these sandwich complexes ($\alpha = 0.7-1.0$);[11,25] so, the more negative cooperativity observed with **1** is probably due to steric interaction between the aryl groups. The greater interaction in toluene appears to reflect an electrostatic contribution from the lower dielectric constant of this solvent. This surprisingly large interaction parameter has a dramatic adverse effect on the stability of ladder complexes in toluene.

**Table 2.** Binding Constants[a] for Monomer **1** and Dimer **2** with Quinuclidine

| solv. | $K$ (monomer **1**) | $K_{11}$ (dimer **2**) | $K_{21}$ (dimer **2**) | $\alpha$ (dimer **2**) |
|---|---|---|---|---|
| PhMe | $(1.8 \pm 0.2) \times 10^6$ | $(2.9 \pm 0.7) \times 10^6$ | $(7.8 \pm 2.0) \times 10^5$ | $1.1 \pm 0.4$ |
| $CHCl_3$ | $(1.0 \pm 0.1) \times 10^5$ | $(2.0 \pm 0.5) \times 10^5$ | $(6.4 \pm 1.6) \times 10^4$ | $1.3 \pm 0.5$ |

[a] In inverse molarity.

We also tested the affinity of compounds **1**−**6** for quinuclidine, a monodentate analogue of DABCO, by spectrophotometric titration. The monomer **1** gives cleanly isosbestic spectra from which binding constants can easily be obtained (Table 2).[22] The titrations of dimer **2** with quinuclidine are nonisosbestic in both chloroform and toluene. Multivariate global factor analysis of the whole series of spectra showed that both titrations can be analyzed in terms of three colored species (free **2** and 1:1 and 1:2 complexes), as shown in Scheme 2, and yielded the binding constants in Table 2. Similar results were also obtained by simplex curve fitting at selected wavelengths, but factor analysis reduces the uncertainty from noise by simultaneously using data at many wavelengths. Here, the interaction parameter $\alpha$ is approximately 1.0. There is no significant cooperativity between quinuclidine binding at the two zinc sites of **2**, and each site has a similar microscopic affinity $K_\mu$ to the monomer **1**. The higher oligomers **3**−**6** also gave nonisosbestic titrations with quinuclidine, but the large number of species present during these titrations made it impossible to analyze the titration curves. We assume that these oligomers bind quinuclidine analogously to the dimer, with each zinc site acting independently with the same microscopic affinity as the porphyrin monomer.

**Probing Ladder Assembly by $^1$H NMR Titration.** Addition of DABCO to solutions of each oligomer **2**−**5**, in $CDCl_3$, results

(23) M and L represent the porphyrin oligomer (or monomer) and DABCO ligand, respectively; $[M]_0$ and $[L]_0$ are the total concentrations of M and L.

(24) Connors, K. A. *Binding Constants*; Wiley: New York, 1987.

(25) Anderson, H. L.; Hunter, C. A.; Meah, M. N.; Sanders, J. K. M. *J. Am. Chem. Soc.* **1990**, *112*, 5780−5789.

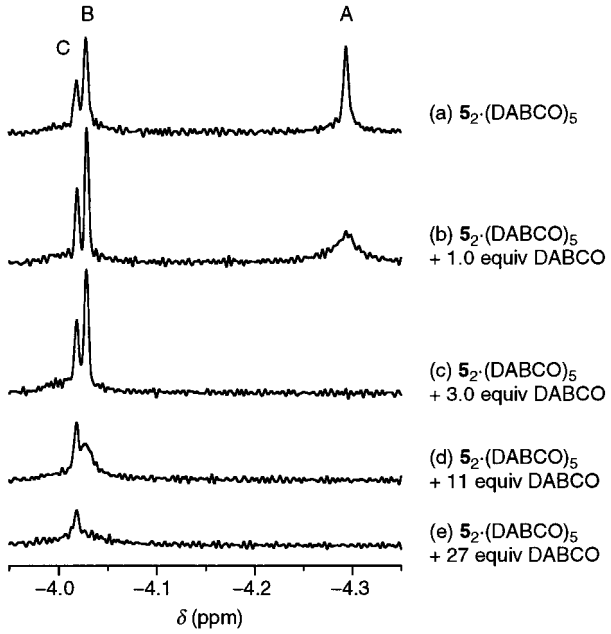


**Figure 2.** $^1$H NMR spectra of the pentamer ladder $\mathbf{5}_2$·(DABCO)$_5$ in the presence of increasing amounts of DABCO showing progressive exchange-broadening of the bound DABCO resonances ($CDCl_3$, 500 MHz, 298 K).

in the appearance of sharp new signals due to the ladder complex (this type of titration could not be carried out with **6** because its solubility is too low). In each case, the equilibrium is in slow exchange when less than the stoichiometric amount of DABCO is added. Ladder formation is an all-or-nothing process: no other complexes are observed apart from the ladder and the unbound oligomer. For example, addition of 1 equiv of DABCO to the tetramer **4** gives a 1:2 mixture of the ladder complex, $\mathbf{4}_2$·(DABCO)$_4$, and unbound **4**. Ladder formation results in an upfield shift of about 0.35 ppm in the aromatic and $\beta$-pyrrole protons, due to the shielding effect of the second strand. As expected, the *ortho*-aryl and *tert*-butyl resonances are split in the ladders, because the faces of the porphyrins become nonequivalent. The bound DABCO resonances appear as sharp singlets around −4 ppm.

When excess DABCO is added to the ladders, the signals start to broaden, and exchange between free and bound DABCO soon becomes fast on the NMR time scale. Exchange between the different DABCO environment in each ladder and free DABCO is fastest for the outermost rungs of the ladder. For example, Figure 2 shows part of the spectrum of $\mathbf{5}_2$·(DABCO)$_5$ in the presence of increasing amounts of DABCO. When there is no excess ligand, this complex gives three DABCO resonances (A−C) with intensities in the ratio 2:2:1 corresponding to the three different ligand environments. As the concentration of DABCO is increased, the signal (A) from the ligands at the ends of the ladder soon broadens out, while the other two signals remain sharp. Then, the next rung (B) starts to go into fast exchange, until only the central rung (C) can be observed. Exchange at the center of the ladder is slowest because it requires the most disruption of the double-strand structure. This process is analogous to the fraying of a DNA duplex; the exchange rates of imine protons in oligodeoxynucleotides[26] and amide protons in α-helical peptides[27] have been previously used to detect fraying. Results presented in the next section show that ladder dissociation (Scheme 3, equilibrium b) is a two-state process: frayed structures do not build up to significant concentrations. The $\mathbf{5}_2$·(DABCO)$_5$ ladder is the predominant species in solution in all of the spectra (a−e) in Figure 2; even after 27 equiv of DABCO have been added, the pentamer is still mostly (>99%) in the form of the ladder complex (as calculated from the equilibrium constant $K_B = 2.7 \times 10^3$ M$^{-4}$; see next section). This NMR experiment allows very low levels of dynamic frayed ladders to be detected.

When DABCO is added to a 1:1 mixture of the dimer **2** and trimer **3**, the only observable complexes are the two homo-ladders $\mathbf{2}_2$·(DABCO)$_2$ and $\mathbf{3}_2$·(DABCO)$_3$; vernier complexes such as $\mathbf{2}_3$·$\mathbf{3}_2$·(DABCO)$_6$ are not formed. Similarly, when DABCO is added to a 1:1 mixture of the butadiyne-linked dimer **2** and its 1,4-diethynylbenzene-linked analogue **2b**,[28] the only

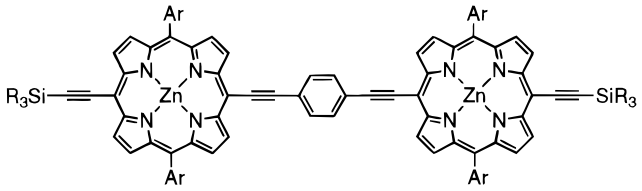


**2b** R = *n*-hexyl; Ar = 3,5-di(*t*-butyl)phenyl

complexes formed are $\mathbf{2}_2$·(DABCO)$_2$ and $\mathbf{2b}_2$·(DABCO)$_2$. This type of narcissistic self-sorting is characteristic of cooperative double-strand formation at thermodynamic equilibrium.[6d,29]

Ladder formation was also observed with Bipy. For example when Bipy is added to the tetramer **4** in $CDCl_3$, sharp signals are observed for the $\mathbf{4}_2$·(Bipy)$_4$ ladder, including two pairs of ligand doublets, as expected. As with DABCO, the equilibrium shifts into fast exchange in the presence of excess ligand.

**Probing Ladder Assembly by UV−Visible Titration.** Addition of DABCO to solutions of oligomers **2**−**5**, in either chloroform or toluene, results in series of isosbestic spectra, showing the formation of ladders $\mathbf{2}_2$·(DABCO)$_2$−$\mathbf{5}_2$·(DABCO)$_5$. With compounds **2**−**4**, ladder formation is instantaneous, whereas with the pentamer **5**, it takes a few minutes; with the hexamer **6**, it takes about 1 h to reach equilibrium, which makes it impractical to carry out this titration with **6**. The titration curves for oligomers **3**−**5** are essentially straight lines (Figure 3). They reach abrupt end points after addition of 1.5, 2.0, and 2.5 equiv of DABCO, respectively, proving the stoichiometries of the $\mathbf{3}_2$·(DABCO)$_3$−$\mathbf{5}_2$·(DABCO)$_5$ complexes. The overall stability constants ($K_F = [M_2L_N]/[M]^2[L]^N$; Scheme 3) are too

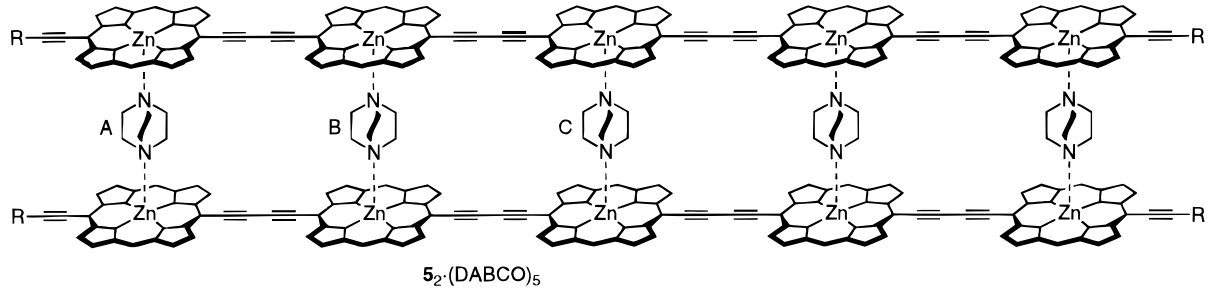


$\mathbf{5}_2$·(DABCO)$_5$

**Scheme 3**

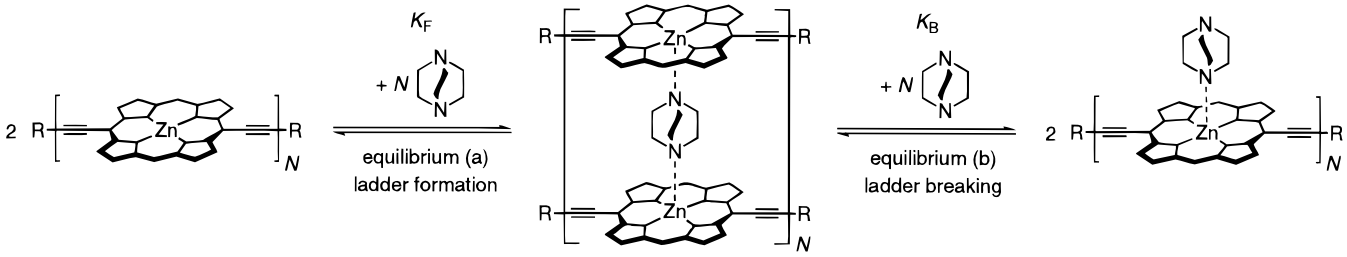


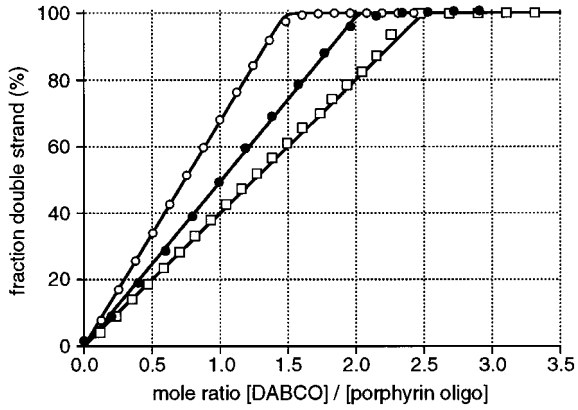


**Figure 3.** Spectrophotometric titration curves for treatment of **3**, (open circles), **4**, (filled circled) and **5** (squares) with DABCO in toluene.

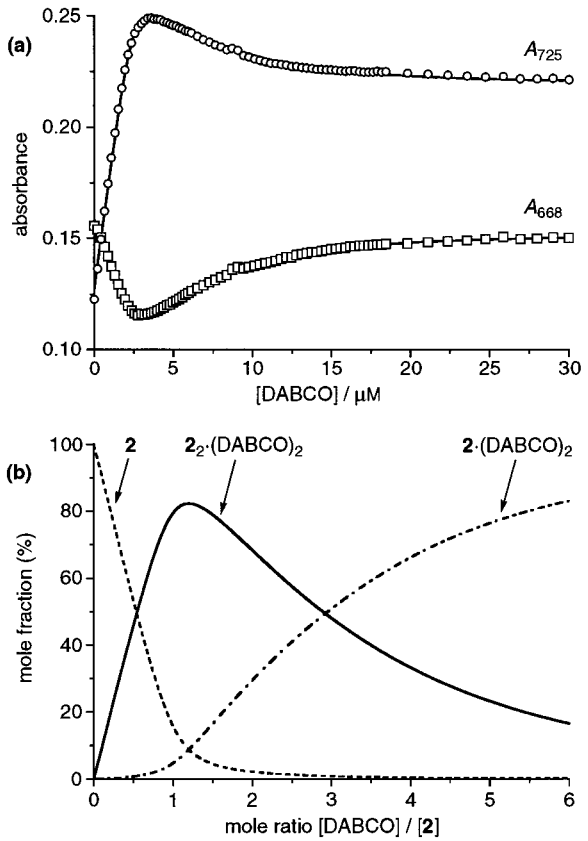


**Figure 4.** Spectrophotometric titration of dimer **2** with DABCO in toluene: (a) change in absorption at two wavelengths (668 and 725 nm) fitted to the calculated curve for the equilibria in Scheme 3; (b) mole fractions of **2**, $\mathbf{2}_2$·(DABCO)$_2$, and **2**·(DABCO)$_2$ during the course of the titration, calculated from global factor analysis of binding curves at all wavelengths in the region 350−850 nm in 1 nm intervals.

strong to measure from these curves. No further changes in the absorption spectra of these ladders are observed until many more equivalents of DABCO are added, when dissociation starts to occur according to equilibrium b in Scheme 3.

The situation with the dimer **2** is more complicated because here $K_F$ is weak enough that, under the dilute conditions of a UV−visible titration, ladder formation does not reach completion with 1 equiv of DABCO. Furthermore, these two-rung ladders soon dissociate in the presence of excess DABCO (particularly in toluene); so, ladder formation never reaches completion. Initially, the titration has sharp isosbestic points, while equilibrium a (Scheme 3) is the main process, but then, the titration enters a nonisosbestic phase before establishing new isosbestic points when equilibrium b dominates in the presence of excess DABCO. We have been unable to adequately analyze these titrations by simplex curve fitting,[30] but global multivariate factor analysis gave reliable results. For example, Figure 4a shows the variation in absorbance at two wavelengths (688 and 725 nm), and Figure 4b shows the concentration profiles obtained by fitting the whole series of spectra to the model shown in Scheme 3, in toluene. The mole fraction of ladder $\mathbf{2}_2$·(DABCO)$_2$ reaches a maximum of 82% after 1.2 equiv of DABCO has been added and falls to 50% with 2.9 equiv of DABCO. The titration curve in chloroform is similar except dissociation is less favorable: the mole fraction of ladder reaches a maximum of 93% after 5 equiv and only falls to 50% after 75 equiv has been added. Values of $K_F$ and $K_B$ are listed in Table 3.

The longer ladders $\mathbf{3}_2$·(DABCO)$_3$−$\mathbf{6}_2$·(DABCO)$_6$ undergo equilibrium b (Scheme 3) in a separate ligand concentration regime from equilibrium a; they give titration spectra with sharp isosbestic points during both phases. For example, Figure 5a shows spectra recorded during the breaking of the hexamer ladder. The clean isosbesticity of these spectra demonstrates that the only colored species present in solution are the ladder $\mathbf{6}_2$·(DABCO)$_6$ and the single-strand complex **6**·(DABCO)$_6$. This is further evidence for the cooperativity of the self-assembly process, and it shows it is valid to analyze these titrations in terms of simple two-state equilibria, which is a valuable simplification. The titration curves for these ladder-breaking equilibria were analyzed using eqs 8−12,[23] which follow from equilibrium b of Scheme 3. $A_i$ and $A_f$ are the initial and limiting

(26) Nonin, S.; Leroy, J.-L.; Guéron, M. *Biochemistry* **1995**, *34*, 10652−10659.

(27) Rohl, C. A.; Baldwin, R. L. *Biochemistry* **1994**, *33*, 7760−7767.

(28) Taylor, P. N.; Wylie, A. P.; Huuskonen, J.; Anderson, H. L. *Angew. Chem. Int. Ed.* **1998**, *37*, 986−989.

(29) Rowan, S. J.; Hamilton, D. G.; Brady, P. A.; Sanders, J. K. M. *J. Am. Chem. Soc.* **1997**, *119*, 2578−2579.

(30) The spectrophotometric titration curves for treatment of **2** with up to 1 equiv of DABCO fit fairly well to the following equation: $2K_F[M]^4 + 4K_F[M]^3([L]_0 - [M]_0) + 2K_F[M]^2([L]_0 - [M]_0)^2 + [M] - [M]_0 = 0$, giving $K_F = (7.0 \pm 5.0) \times 10^{19}$ M$^{-3}$ in toluene and $(2.0 \pm 0.8) \times 10^{18}$ M$^{-3}$ in chloroform.[23]

**Table 3.** Binding Constants for Porphyrin Oligomers and DABCO

| solvent | $N$ | $K_B/M^{(1-N)}$ | $K_F/M^{-(1+N)}$ | $c_{50}/M$ |
|---|---|---|---|---|
| PhMe | 1 | $(6.7 \pm 0.6) \times 10^2$ | $(4.9 \pm 0.5) \times 10^9$ [a] | $7.1 \times 10^{-6}$ |
| PhMe | 2 | $(2.0 \pm 0.3) \times 10^5$ | $(9.7 \pm 2.8) \times 10^{19}$ [a] | $8.6 \times 10^{-8}$ |
| | | | $(5.2 \pm 1.5) \times 10^{19}$ [b] | |
| PhMe | 3 | $(6.8 \pm 2.0) \times 10^7$ | $(5.0 \pm 2.0) \times 10^{29}$ [b] | $1.2 \times 10^{-8}$ |
| PhMe | 4 | $(1.5 \pm 0.6) \times 10^{10}$ | $(7.3 \pm 3.5) \times 10^{39}$ [b] | $2.7 \times 10^{-9}$ |
| PhMe | 5 | $(1.6 \pm 0.8) \times 10^{12}$ | $(2.2 \pm 1.3) \times 10^{50}$ [b] | $8.4 \times 10^{-10}$ |
| PhMe | 6 | $(3.4 \pm 2.0) \times 10^{14}$ | $(3.4 \pm 2.3) \times 10^{60}$ [b] | $4.0 \times 10^{-10}$ |
| $CHCl_3$ | 1 | $20 \pm 2$ | $(4.9 \pm 0.5) \times 10^8$ [a] | $2.3 \times 10^{-5}$ |
| $CHCl_3$ | 2 | $107 \pm 21$ | $(1.8 \pm 0.5) \times 10^{18}$ [a] | $3.3 \times 10^{-7}$ |
| | | | $(8.6 \pm 2.5) \times 10^{17}$ [b] | |
| $CHCl_3$ | 3 | $(5.7 \pm 1.7) \times 10^2$ | $(1.6 \pm 0.6) \times 10^{27}$ [b] | $4.9 \times 10^{-8}$ |
| $CHCl_3$ | 4 | $(5.0 \pm 2.0) \times 10^2$ | $(1.7 \pm 0.8) \times 10^{37}$ [b] | $9.0 \times 10^{-9}$ |
| $CHCl_3$ | 5 | $(2.7 \pm 1.4) \times 10^3$ | $(3.0 \pm 1.8) \times 10^{46}$ [b] | $3.7 \times 10^{-9}$ |
| $CHCl_3$ | 6 | $(2.6 \pm 1.6) \times 10^3$ | $(3.0 \pm 2.0) \times 10^{56}$ [b] | $1.5 \times 10^{-9}$ |

[a] Measured directly. [b] Calculated from $K_B$ by eq 13 using $K_\mu$ of monomer **1**.

absorbances; $A_{obs}$ is the absorbance at any point in the titration.

$$K_B = [ML_N]^2/([M_2L_N][L]^N) \quad (8)$$

$$[M]_0 = 2[M_2L_N] + [ML_N] \quad (9)$$

$$[L]_0 = [L] + N[M_2L_N] + N[ML_N] \quad (10)$$

$$K_B[M_2L_N]\{[L]_0 + N([M_2L_N] - [M]_0)\}^N - (2[M_2L_N] - [M]_0)^2 = 0 \quad (11)$$

$$A_{obs} = (2A_i[M_2L_N] + A_f[ML_N])/[M]_0 \quad (12)$$

We assume that the concentration of unbound porphyrin oligomer is negligible ([M] $\approx$ 0) in the concentration regime of these titrations, as demonstrated by the curves in Figure 3. Values of $K_B$ from these titrations are listed in Table 3.

As the ladders become longer, they become increasingly reluctant to open up into single-strand complexes. The titration curve for interaction of excess DABCO with the hexamer ladder is shown in Figure 5b. In toluene, the amount of DABCO required to break 50% of the ladders into single strands is 1200 equiv for the hexamer, compared to only 2.9 equiv for the dimer! The breaking curve for the hexamer is also highly sigmoidal, as predicted by the theoretical model of eqs 8−11. As the ladders become longer, their dissociation curves become more sigmoidal, as reflected by the Hill plots[24] in Figure 6. The Hill coefficients $n_H$ increase from 1.3 to 4.0 with increasing ladder length, reflecting the increasing cooperativity of ladder assembly and dissociation.[31] Hill coefficients of up to 1.75 have been recorded for the assembly of copper(I) trihelicates.[6a]

**Determination of Ladder Stability.** Although the stability constants of the ladders, $K_F$, are too high to measure directly (except for the dimer) they can be calculated from the equilibrium constants for breaking the ladders with excess DABCO, $K_B$, using the thermodynamic cycle shown in Scheme 4, which leads to eq 13.

$$K_F = (2K_\mu)^{2N}/K_B \quad (13)$$

$K_\mu$ is the microscopic binding constant for each zinc site on the porphyrin oligomer for one end of DABCO. We assume that

(31) Hill coefficients are most commonly used to measure cooperativity in the binding of monovalent ligands L to a multivalent receptors M to give a $ML_N$ complexes, but they have also been applied to multiple-strand formation equilibria;[3,6a] they allow cooperativity to be empirically quantified even when the binding stoichiometry is poorly defined.

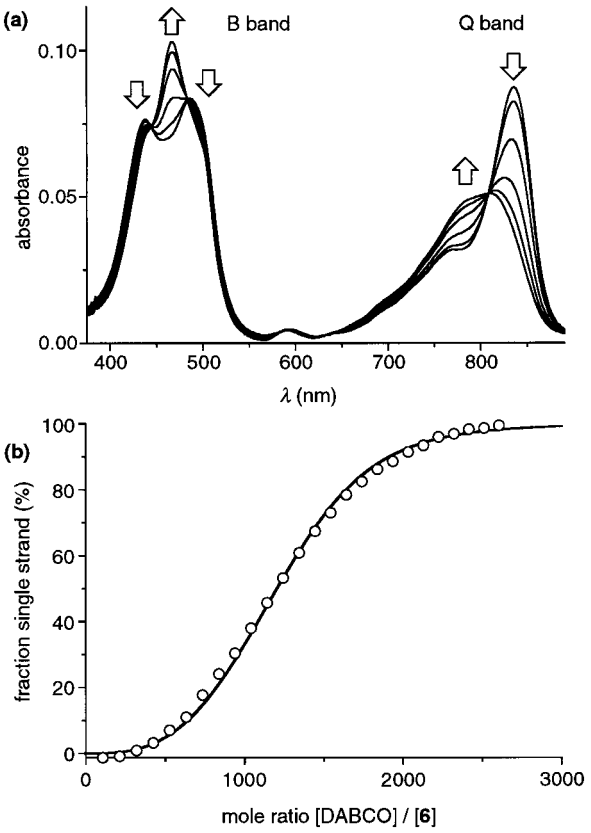


**Figure 5.** Titration of the hexamer ladder $\mathbf{6}_2$·$(DABCO)_6$ with excess DABCO in toluene ($[\mathbf{6}]_0 = 2.5 \times 10^{-7}$ M): (a) selected absorption spectra during the course of the titration and (b) complexation isotherm, showing sigmoidal rise in the mole fraction of the $\mathbf{6}$·$(DABCO)_6$ single-strand complex, fitted to the calculated curve for eqs 8−12.

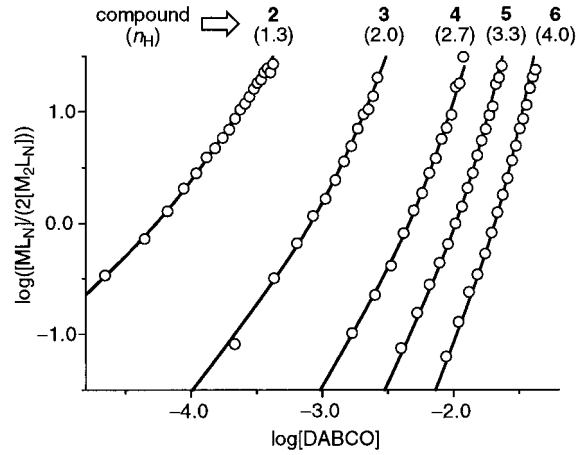


**Figure 6.** Hill plots for treatment of the ladders $\mathbf{2}_2$·$(DABCO)_2$−$\mathbf{6}_2$·$(DABCO)_6$ with excess DABCO from spectrophotometric titration data, fitted to the calculated curves from eqs 8−12. The Hill coefficient $n_H$ is defined as the gradient of the curve at $\log([ML_N]/(2[M_2L_N])) = 0$.

for all of the oligomers **2**−**6** $K_\mu$ is half the stability constant of **1**·DABCO (Scheme 1; $K_\mu = 0.5K_{11} = 9.0 \times 10^5$ $M^{-1}$ in toluene and $4.9 \times 10^4$ $M^{-1}$ in chloroform) and that all of the sites on an oligomer behave independently when they bind just one end of DABCO. Two independent lines of evidence validate this assumption, in both toluene and chloroform: (i) quinuclidine binds independently to the two sites of **2** with the same microscopic binding constant as **1** (Scheme 2), and (ii) in the case of the dimer **2**, where $K_F$ and $K_B$ can be measured directly, eq 13 is found to be a valid approximation in both solvents. Values of $K_F$ calculated from $K_B$ and $K_\mu$ using eq 13 are listed

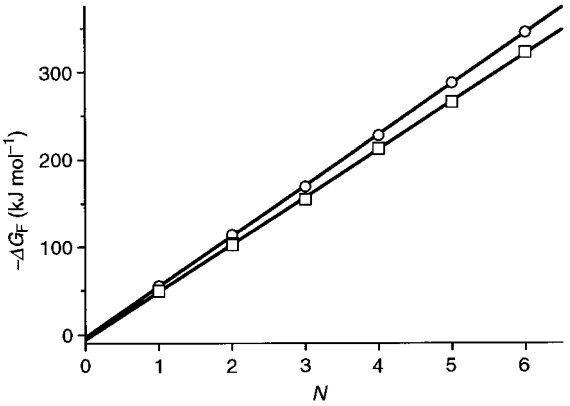


**Figure 7.** Gibbs free energy of ladders formation ($\Delta G_F = -RT \ln K_F$) plotted against the number of porphyrins in the oligomer $N$, in toluene (circles) and chloroform (squares).

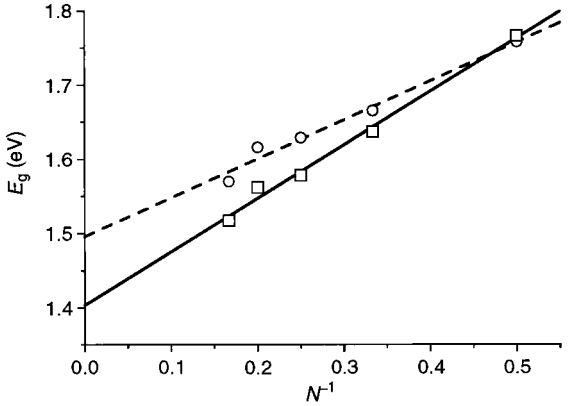


**Figure 8.** Plot of optical gap $E_g$ (from peak Q-band absorption) against reciprocal chain length $N^{-1}$, for single-strand DABCO complexes (circles) and ladders (squares) in toluene.

**Scheme 4**

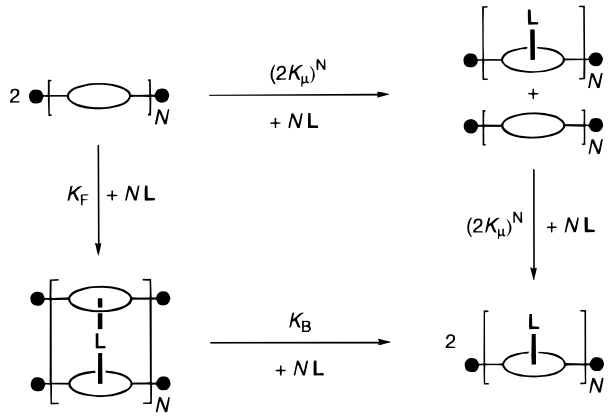


in Table 3. It is difficult to compare the stabilities of ladders with different lengths because the dimensions of $K_F$ vary with $N$ ($K_F$ has units [molar]$^{-(N+1)}$). One way around this problem is to calculate the concentration, $c_{50}$, at which each ladder is 50% dissociated into single strands simply by dilution (at the correct 2:$N$ stoichiometry) using eq 14.

$$c_{50} = \frac{1}{\sqrt[(N+1)]{4K_F N^N}} \qquad (14)$$

The values of $c_{50}$ calculated from $K_F$ (Table 3) show that as the ladders become longer they become stable to lower concentrations despite the fact that they are higher order assemblies. The stabilities of the ladders become increasingly concentration dependent, and this almost compensates for the increasing $K_F$.

Gibbs free energies of ladder formation ($\Delta G_F = -RT \ln K_F$) are compared in Figure 7. Plots of $\Delta G_F$ versus $N$ in both chloroform and toluene give remarkably straight lines. Adding each new rung to the ladder increases the free energy by the same amount. The intercepts at $N = 0$ correspond to unfavorable entropies of ladder initiation of 11 J K$^{-1}$ mol$^{-1}$ in toluene and 20 J K$^{-1}$ mol$^{-1}$ in chloroform. Similar linear free energy relationships (with positive intercepts at $N = 0$) are found for DNA duplex formation.[2b]

**Change in Conjugation between Single- and Double-Strand Oligomers.** Ladder formation was anticipated to favor conformations in which neighboring porphyrin macrocycles are coplanar and thus to increase the interporphyrin electronic conjugation. The changes in the UV−visible spectra accompanying breaking of ladder complexes with excess DABCO (Scheme 3b) demonstrate that there is indeed increased electronic overlap in the ladder complexes. For example, Figure 5a shows that the hexamer ladder has a more redshifted Q-band and a more widely split B-band than those of the single-strand complex. There is no change in the local coordination environment of the zinc porphyrin unit during this ladder-breaking process. Weak interstrand exciton coupling between the face-to-face porphyrins in the ladder complex must cause a slight blueshift in the absorption.[32] So the redshifted Q-band and the broader B-band in the ladder complex are clear indications of a reduction in the interporphyrin dihedral angle. Figure 8 shows how the transition energy, or optical gap $E_g$, varies with the reciprocal of the number of porphyrin units in the oligomer $N^{-1}$ for ladders and for single-strand complexes.[12] The steeper curve for the ladder complexes shows that they are more conjugated. It is interesting that no increase in conjugation is evident in the dimer ladder $\mathbf{2}_2$·(DABCO)$_2$ when compared with that in **2**·(DABCO)$_2$; this indicates that planarization requires at least three rungs in the ladder.

The increase in interporphyrin conjugation accompanying ladder formation is probably less than what would be expected if the unbound oligomers had completely free rotation about the butadiyne links, suggesting that the distribution of dihedral angles is weighted toward more planar, more conjugated, conformers, even without ladder formation, as indicated by work on related systems.[12,13,33]

Comparison of the UV−visible absorption spectrum of the 4,4′-bipyridyl ladder $\mathbf{4}_2$·(Bipy)$_4$ with that of $\mathbf{4}_2$·(DABCO)$_4$ confirms that interstrand exciton coupling is not a significant factor in these spectra. The shapes of the B-bands of the two complexes are very similar, with that of $\mathbf{4}_2$·(Bipy)$_4$ redshifted by only 2 nm. However, the spectrum of $\mathbf{4}_2$·(Bipy)$_4$ is noticeably sharper, particularly in the Q-band, and its Q-band is redshifted by 16 nm, which indicates that this Bipy ladder is more ordered and more planar, perhaps because the strands are far enough apart to avoid steric interactions between the aryl groups.

## Conclusions

Ladder formation−dissociation equilibria exhibit the following characteristics of cooperative self-assembly:

(32) Hunter, C. A.; Sanders, J. K. M.; Stone, A. J. *Chem. Phys.* **1989**, *133*, 395−404. Hunter, C. A.; Meah, M. N.; Sanders J. K. M. *J. Am. Chem. Soc.* **1990**, *112*, 5773−5780. Mak, C. C.; Bampos, N.; Sanders, J. K. M. *Angew. Chem., Int. Ed. Engl.* **1998**, *37*, 3020−3023. Mak, C. C.; Pomeranc, D.; Montalti, M.; Prodi, L.; Sanders, J. K. M. *Chem. Commun.* **1999**, 1083−1084.

(33) Lin, V. S.-Y.; Therien, M. J. *Chem. Eur. J.* **1995**, *1*, 645−651. Stranger, R.; McGrady, J. E.; Arnold, D. P.; Lane, I.; Heath, G. A. *Inorg. Chem.* **1996**, *35*, 7791−7797. Kumble, R.; Palese, S.; Lin, V. S.-Y.; Therien M. J.; Hochstrasser, R. M. *J. Am. Chem. Soc.* **1998**, *120*, 11489−11498. Wilson, G. S.; Anderson, H. L. *Chem. Commun.* **1999**, 1539−1540.

**a. All-or-Nothing Formation and Dissociation.** If significant amounts of partially formed ladders were formed, they would have been observed by $^1$H NMR (because ladder assembly is in slow exchange) and the UV−visible spectra would have been nonisosbestic. There is no such sign of these intermediates. However, low concentrations of partially formed frayed ladders can be detected indirectly through the different exchange rates of the different rungs of the ladders with excess DABCO.

**b. Narcissistic Self-Sorting.** $^1$H NMR titrations show that mixtures of **2**, **3**, and DABCO give only $\mathbf{2}_2\cdot(\mathrm{DABCO})_2$ and $\mathbf{3}_2\cdot(\mathrm{DABCO})_3$, and mixtures of **2**, **2b**, and DABCO give only $\mathbf{2}_2\cdot(\mathrm{DABCO})_2$ and $\mathbf{2b}_2\cdot(\mathrm{DABCO})_2$.

**c. Sigmoidal Binding Curves.** The UV−visible titration isotherms for ladder dissociation become increasingly sigmoidal as the ladders become longer.[34]

**d. Large Hill Coefficients.** The Hill coefficients $n_H$ for ladder dissociation increase gradually from the dimer to the hexamer and are all greater than unity. In all cases, the Hill coefficients have the theoretically predicted values for the two-state equilibrium of Scheme 3b to within two significant figures.

**e. Increasing Ladder Stability with Increasing Length.** The Gibbs free energy for ladder formation has a linear length dependence, as has been observed in DNA oligomers. This is manifested by the increasingly high concentrations of excess DABCO required to break the ladders into single-strand complexes.

**f. Self-Assembly Constrains the Conformation.** The increased planarity and $\pi$-overlap in the ladder structures, compared to single-strand complexes, is apparent from the increased splitting in the Q-band and from the reduction in HOMO−LUMO gap. This is analogous to the way nature uses self-assembly to control tertiary structure. It remains to be discovered whether this effect is large enough to be useful in the optimization of these materials for nonlinear optics, but it does at least make their electronic spectra highly sensitive to conformational changes. The dramatic changes in the absorption spectra that accompany ladder formation and dissociation have enabled us to probe these equilibria in a level of detail that would probably not have been possible with nonconjugated analogues.

## Experimental Section

**Materials.** Compounds **1**−**6** and **2b** were prepared as described previously;[12,28] full experimental details of this synthetic work are provided in the Supporting Information. Deutero-chloroform was deacidified by standing over potassium carbonate. Chloroform for UV−visible titrations contained 0.5% ethanol stabilizer, and this amount of ethanol was also added to $CDCl_3$ for quantitative NMR titrations, so that NMR and spectrophotometric results can be directly compared. Toluene was distilled from calcium hydride. Deutero-toluene, DABCO, and quinuclidine were used as supplied.

**Instrumentation.** $^1$H NMR titrations were carried out on a Bruker AM-500 spectrometer (500 MHz). UV−visible spectra were recorded on a Perkin-Elmer Lambda 20 instrument.

**Methods.** $^1$H NMR and UV−visible titrations were performed by adding solutions of the ligand to a solution of the porphyrin in either a 5 mm NMR tube or a 1 cm path length quartz cuvette, using microliter syringes. The porphyrin was present in the ligand at the same concentration as that in the NMR tube or cuvette, to avoid dilution effects. All spectra and titrations were performed at 298 K (except those for van't Hoff plots[22]). UV−visible titrations were carried out with peak absorbances in the range 0.1−1.0, which corresponds to a porphyrin concentration of ca. $10^{-6}$ M. $^1$H NMR titrations were carried out at a porphyrin concentration of ca. $10^{-3}$ M.

**Data Analysis.** $^1$H NMR titration curves were analyzed by fitting the experimental data to the theoretically expected curve (see text) using a simplex nonlinear curve-fitting program, using a combination of bisection and the Newton−Raphson method to iteratively solve polynomial equilibrium expressions.[35] UV−visible spectrophotometric titrations were analyzed both by using this simplex method (at several wavelengths in turn) and by fitting the whole series of spectra at 1 nm intervals using the software SPECFIT, ver 2.11 (from Spectrum Software Associates, P.O. Box 4494, Chapel Hill, NC 27515-4494), which uses a global analysis system with expanded factor analysis and Marquardt least-squares minimization to obtain globally optimized parameters.[18] The two methods gave very similar results in all cases, although the second method is certainly more accurate, and in one case (the full equilibrium of **2**, $\mathbf{2}_2\cdot(\mathrm{DABCO})_2$, $\mathbf{2}\cdot(\mathrm{DABCO})_2$, and DABCO), this was the only applicable method of analysis.

Measurements of simple 1:1 binding constants were found to be reproducible to within 10%. Errors in higher order binding constants are correspondingly higher, because they are more sensitive to inaccuracies in concentration and absorption or chemical shift; values of $K_B$ with units of molarity to the power of $(1 - N)$ have errors of approximately $N \times 10\%$. These estimates of the errors are much higher that those from statistical analysis of the data from SPECFIT. The standard deviation $\sigma$ in quantities such as $K_F$ and $\alpha$, which are derived from $n$ experimental binding constants (with standard deviation $\sigma_i$), were calculated using eq 15.[36]

$$\sigma = \sqrt{\sum_{i=1}^{n} \sigma_i^2} \qquad (15)$$

**Acknowledgment.** This work was generously supported by the Engineering and Physical Research Council (EPSRC), U.K. We thank the EPSRC mass spectrometry service (Swansea) for FAB mass spectra.

**Supporting Information Available:** Experimental procedures for the synthesis of compounds **1**−**6**. This material is available free of charge via the Internet at http://pubs.acs.org.

JA992821D

(34) Ladder formation curves would also be sigmoidal if titrations were carried out at a sufficiently low concentration.

(35) Press, W. H.; Flannery, B. P.; Teukolsky, S. A.; Vetterling, W. T. *Numerical Recipes in Pascal*; Cambridge University: Cambridge, U.K., 1989.

(36) Crumpler, T. B.; Yoe, J. H. *Chemical Computation and Errors*; J. Wiley: New York, 1940; pp 180−183.